Science
AAAS

Docking in Metal-Organic Frameworks
Qiaowei Li, *et al.*
Science **325**, 855 (2009);
DOI: 10.1126/science.1175441

This overpotential should be affected by the catalytic activity of the electrode and, thus, the size of the Ni particles in the anode should also affect the cell performance, especially at lower operating temperature.

The outstanding performance of cell A seems to arise from the improvement of the anode microstructure (Ni particle size below 100 nm). The open-circuit voltages slightly decreased from 1.1 V for cell C to 1.0 V for cell A as sintering temperature decreased from 1400° to 1250°C. This change possibly relates to the density of the electrolyte. Bundling of the cells, stack design, and modularization are other challenges that need to be overcome for the realization of high-performance SOFC systems.

References and Notes

1. N. Q. Minh, *J. Am. Ceram. Soc.* **76**, 563 (1993).
2. O. Yamamoto, *Electrochim. Acta* **45**, 2423 (2000).
3. S. C. Singhal, *Solid State Ion.* **152–153**, 405 (2002).
4. B. C. H. Steele, A. Heinzel, *Nature* **414**, 345 (2001).
5. H. Yokokawa, N. Sakai, T. Horita, K. Yamaji, M. E. Brito, *MRS Bull.* **30**, 591 (2005).
6. J. Yan, H. Matsumoto, M. Enoki, T. Ishihara, *Electrochem. Solid-State Lett.* **8**, A389 (2005).
7. Z. Shao, S. M. Haile, *Nature* **431**, 170 (2004).
8. S. Tao, J. T. S. Irvine, *Nat. Mater.* **2**, 320 (2003).
9. H. Huang *et al.*, *J. Electrochem. Soc.* **154**, B20 (2007).
10. K. Eguchi, T. Setoguchi, T. Inoue, H. Arai, *Solid State Ion.* **52**, 165 (1992).
11. T. Hibino *et al.*, *Electrochem. Solid-State Lett.* **5**, A242 (2002).
12. E. D. Wachsman, *Solid State Ion.* **152–153**, 657 (2002).
13. R. T. Leah, N. P. Brandon, P. Aguiar, *J. Power Sources* **145**, 336 (2005).
14. N. M. Sammes, Y. Du, R. Bove, *J. Power Sources* **145**, 428 (2005).
15. K. Kendall, M. Palin, *J. Power Sources* **71**, 268 (1998).
16. K. Yashiro *et al.*, *Electrochemistry* **70**, 958 (2002).
17. T. Suzuki, T. Yamaguchi, Y. Fujishiro, M. Awano, *J. Power Sources* **171**, 92 (2007).
18. T. Suzuki, Y. Funahashi, T. Yamaguchi, Y. Fujishiro, M. Awano, *Electrochem. Solid-State Lett.* **10**, A177 (2007).
19. S. de Souza, S. J. Visco, L. C. DeJohnge, *J. Electrochem. Soc.* **144**, L35 (1997).
20. S. P. Simner *et al.*, *Electrochem. Solid-State Lett.* **5**, A173 (2002).
21. Materials and methods are available as supporting material on *Science* Online.
22. A. Gunji *et al.*, *J. Power Sources* **131**, 285 (2004).
23. Z. Wang *et al.*, *Mater. Lett.* **59**, 2579 (2005).
24. S. H. Chan, K. A. Khor, Z. T. Xia, *J. Power Sources* **93**, 130 (2001).
25. W. Lehnert, J. Meusinger, F. Thom, *J. Power Sources* **87**, 57 (2000).

26. This work was supported by the New Energy and Industrial Technology Development Organization as part of the Advanced Ceramic Reactor Project. The authors have submitted a patent related to low-temperature-operable microtubular SOFCs.

Supporting Online Material

www.sciencemag.org/cgi/content/full/325/5942/852/DC1
Materials and Methods

18 May 2009; accepted 23 June 2009
10.1126/science.1176404

Docking in Metal-Organic Frameworks

Qiaowei Li,[1]* Wenyu Zhang,[1]* Ognjen Š. Miljanić,[1] Chi-Hau Sue,[2] Yan-Li Zhao,[2] Lihua Liu,[2] Carolyn B. Knobler,[1] J. Fraser Stoddart,[2] Omar M. Yaghi[1]

The use of metal-organic frameworks (MOFs) so far has largely relied on nonspecific binding interactions to host small molecular guests. We used long organic struts (~2 nanometers) incorporating 34- and 36-membered macrocyclic polyethers as recognition modules in the construction of several crystalline primitive cubic frameworks that engage in specific binding in a way not observed in passive, open reticulated geometries. MOF-1001 is capable of docking paraquat dication (PQT^{2+}) guests within the macrocycles in a stereoelectronically controlled fashion. This act of specific complexation yields quantitatively the corresponding MOF-1001 pseudorotaxanes, as confirmed by x-ray diffraction and by solid- and solution-state nuclear magnetic resonance spectroscopic studies performed on MOF-1001, its pseudorotaxanes, and their molecular strut precursors. A control experiment involving the attempted inclusion of PQT^{2+} inside a framework (MOF-177) devoid of polyether struts showed negligible uptake of PQT^{2+}, indicating the importance of the macrocyclic polyether in PQT^{2+} docking.

The concept of architectural domains that operate independently, yet are interconnected, is common in biology but difficult to achieve in synthetic materials. We believe that this concept offers a useful strategy for achieving materials with higher complexity. We have focused our attention on the design and synthesis of porous crystals composed of several architectural domains, one of which is capable of docking molecules in a manner akin to the well-known docking of drug molecules.

Our design takes advantage of the emerging chemistry of metal-organic frameworks (MOFs) (*1*–*3*), which has been used effectively to assemble components with simple constitutions—specifically, organic struts and inorganic joints—into three-dimensionally ordered structures. The vast majority of porous MOFs prepared thus far can be regarded (Fig. 1) as having two important architectural domains: (i) the pore aperture, which is responsible for the shape- and size-selective binding of incoming molecules, and (ii) the internal surface of the pores, onto which gases or small molecules can be compacted and distributed with simple interaction sites covering the struts and joints; in some cases, the interaction is with open metal sites. These two domains are called the sorting domain (*2*) and the coverage domain (*4*–*8*), respectively.

The synthesis of more complex MOFs, where more than two domains are present, has remained unexplored. Here, we show how molecular recognition components, much used in supramolecular chemistry (*9*, *10*), can be integrated in a modular fashion into struts of MOFs, thereby creating recognition sites into which incoming guests will dock in a highly specific manner with stereoelectronic control. This third architectural domain—the active domain—combines shape, size, and electronic elements in the recognition of incoming guests, and brings order to otherwise highly disordered guests in conventional MOFs. Hence, this chemistry describes a class of MOFs with a level of complexity higher than that of known open reticulated geometries (*1*).

We used the primitive cubic topology of the archetypical MOF-5 (*11*), in which benzene struts are joined by $Zn_4O(CO_2)_6$ cluster joints, as the target for our design. Initially, we demonstrated the feasibility of using the long 1/4DMBDA (**1**) to make MOF-1000 (*12*), which has the MOF-5 topology, albeit quadruply interpenetrated (Fig. 2A). This approach was extended to the more complex struts BPP34C10DA (**2**) and 1/5DNPPP36C10DA (**3**), which are known to act as electron-rich receptors for electron-deficient substrates (*13*), to make the corresponding MOF-1001A, MOF-1001, and MOF-1002 (Fig. 2, B to D). Each of the crown ether receptors in MOF-1001 is accessible, as evidenced by the docking of the paraquat dication (PQT^{2+}) at every one of the receptor sites (see below). In contrast to known MOFs, where the frameworks are used mainly as passive platforms for the adsorption of gases and molecules, MOF-1001 not only has active components in precise recognition sites but also, by virtue of the openness of its structure, allows substrates to diffuse freely from solution, through the pores, and finally dock in these active domains.

Crystals of MOF-1000 (*14*) (Fig. 2A and Fig. 3A) were obtained by mixing a solution of strut **1** (*15*) with $Zn(NO_3)_2{\cdot}4H_2O$ in *N*,*N*-diethylformamide under conditions previously used in the synthesis of MOF-5 (*5*, *11*). Its crystal structure displays the same structural topology as does MOF-5. It is found to be four-fold interpenetrated because of the length and slender nature of the strut; the distance between the two carboxylate carbon atoms is 19.3 Å. The successful crystallization of MOF-1000 confirmed the practicality of creating MOFs with higher complexity by means of this synthetic protocol.

Struts **2** and **3** respectively contain 34- and 36-membered polyether rings, which have been extensively used (*13*) as receptors for a wide range of electron-deficient substrates. These struts are ideally suited as molecular recognition modules for making MOFs. Strut **2** was prepared by means of a convergent synthetic approach (*14*) and was used under conditions similar to those used in the synthesis of MOF-1000 to yield MOF-1001A

[1]Department of Chemistry and Biochemistry, University of California, Los Angeles, CA 90095, USA. [2]Department of Chemistry, Northwestern University, Evanston, IL 60208, USA.

*To whom correspondence should be addressed. E-mail: qwli@chem.ucla.edu (Q.L.); wyzhang@chem.ucla.edu (W.Z.)

and MOF-1001 (*14*). The crystal structure of MOF-1001A is a triply interpenetrating framework (Fig. 2B and Fig. 3B), whereas that of MOF-1001 is the corresponding noninterpenetrating form (Fig. 2C and Fig. 3C); both have the MOF-5–type topology. The existence of MOF-1001A, despite its occasional appearance as a minor product, validates indirectly the high porosity of MOF-1001. The sheer openness of the structure, however, led us to further optimize the reaction conditions to successfully obtain MOF-1001 as a pure phase (*14*). MOF-1001 has $Fm\bar{3}m$

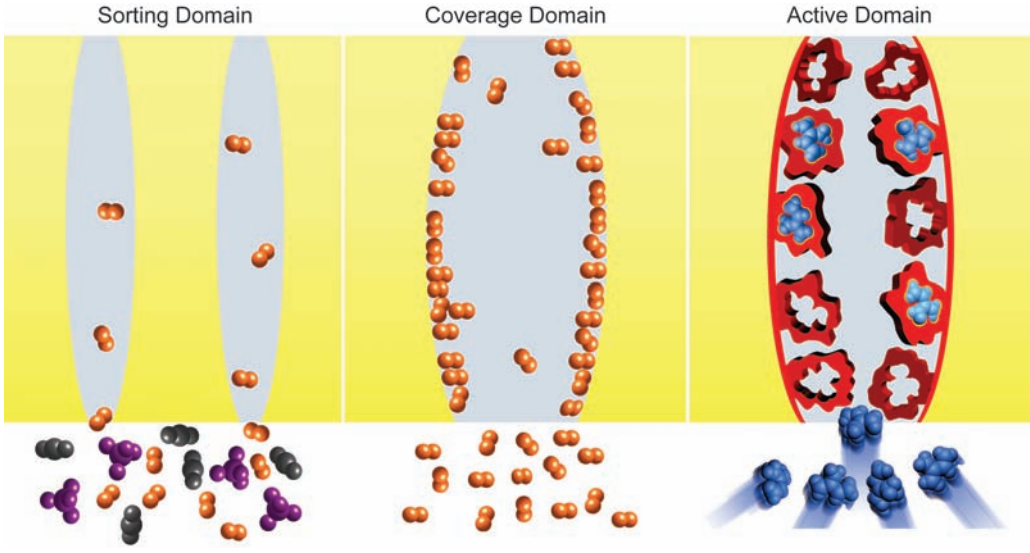

Fig. 1. Classification of the different porous domains in metal-organic frameworks. In the sorting domain, guest molecules are selected according to their size at the orifices of the pores. The entry of H_2 (orange) and concomitant exclusion of CO_2 (black) and CH_4 (purple) reflects the sieve-like action at the entrances to the pores. In the coverage domain, the guest molecules along the walls of the pores are disordered on account of their weak nonspecific interactions with the framework surrounding the pores. By contrast, the active domain has built-in recognition sites that help to maneuver and dock incoming guests in a highly selective and stereoelectronically controlled manner. These recognition sites (red) could be π-electron–rich and, as such, would seek out π-electron–deficient substrates (blue).

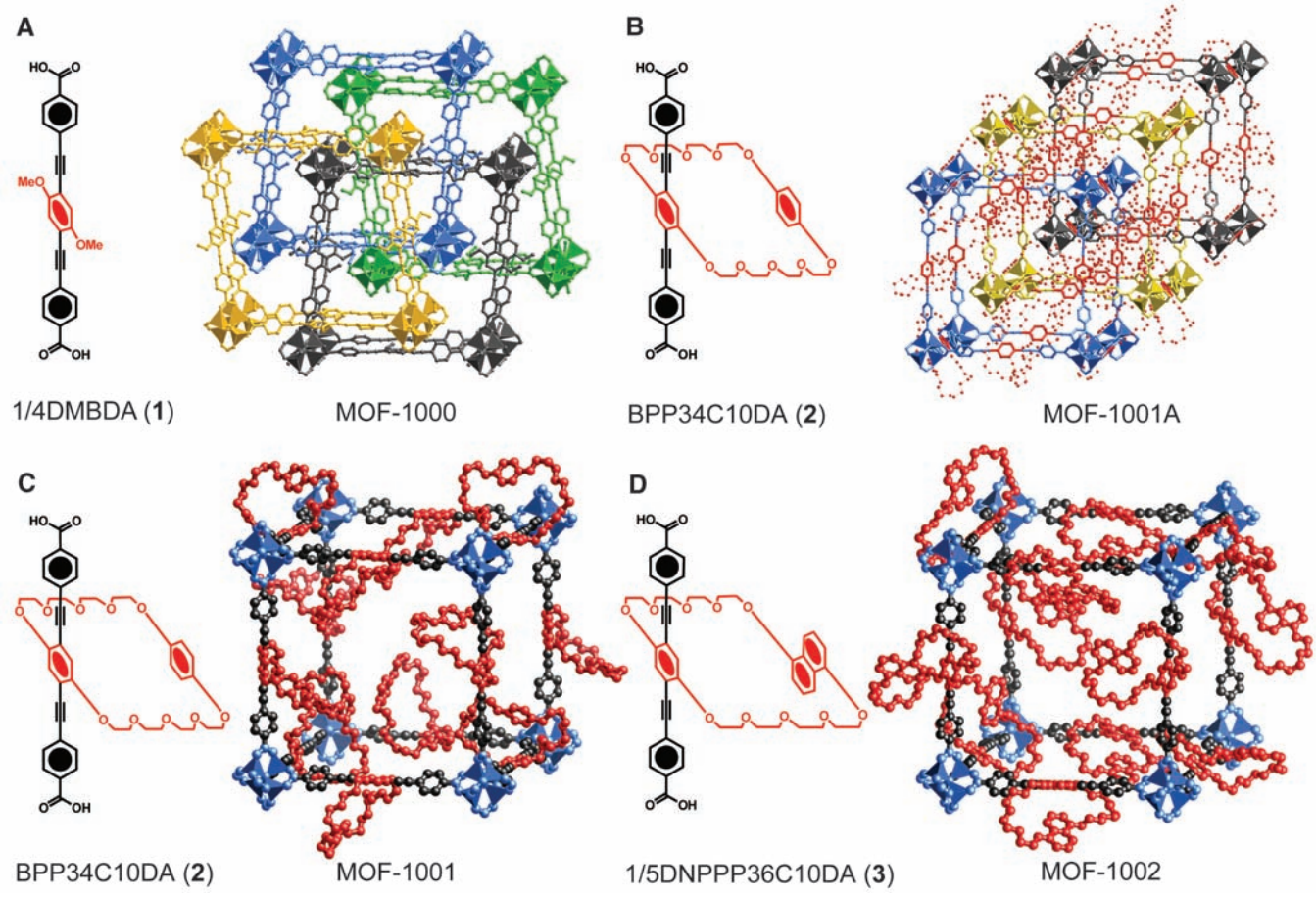

Fig. 2. Ball-and-stick drawings of single-crystal structures of MOF-1000, MOF-1001A, MOF-1001, MOF-1002, and their corresponding organic struts. Strut **1** was used to obtain MOF-1000 (**A**), which has a four-fold interpenetrating structure with different frameworks shown in four different colors. The crystal structure of MOF-1001A from strut **2** (**B**) is a triply interpenetrating cubic structure (shown in blue, gold, and gray), with polyethers represented by red balls and wires. (**C** and **D**) MOF-1001 from strut **2** (C) and MOF-1002 from strut **3** (D) share an identical cubic framework backbone, and crown ethers are placed precisely throughout the whole framework [$Zn_4O(CO_2)_6$ polyhedra, blue; organic struts, gray; crown ethers, red]. Crown ethers in all the structures were modeled by Cerius[2]. All hydrogen atoms have been omitted for clarity.

symmetry, with an exceptionally large unit cell parameter a = 52.93 Å.

We then extended the methodology to the synthesis of MOF-1002 (Fig. 2D and Fig. 3D) by using the 1,5-dioxynaphthalene–containing strut **3,** which was produced by a divergent synthetic route (*14*). Single-crystal x-ray diffraction studies (*14*) indicate that MOF-1002 shares an identical cubic backbone with MOF-1001, affirming the generality of such a methodology for building a variety of crystalline structures with long struts capable of molecular recognition.

Calculations of the volumes of open space within the MOF structures confirmed the highly open nature of these crystals (86.9% space unoccupied by MOF-1001 framework atoms, as assessed by a model using the program Cerius^2, version 4.2). The inherent flexibility of the macrocyclic polyether substructure was evident from the single-crystal x-ray analysis of MOF-1001. The bismethylenedioxy units of the tetraethylene glycol loops in the substructure are found to be highly disordered. Nonetheless, the positions of all the atoms in the inorganic joints and the rigid backbone of the links are unambiguous, as judged by comparison of the resulting bond distances and angles with the model structure (*16*). On the basis of the overall geometry and stoichiometry of the MOF framework, we can conclude that the crown ether receptors—capable of the complexation behavior required (*17*) for molecular recognition—are integrated precisely and periodically inside a robust framework. Thus, the extended framework provides the basis for their strategic placement so that they are exposed to the maximum accessibility to guests in three-dimensional space.

To date, a number of reports (*18*–*20*) have appeared on the synthesis and structure of hybrid organic-inorganic compounds with macrocycles and mechanically interlocking components. The MOFs presented here combine the precise positioning of the active domains with docking as an expression of molecular recognition. This property was revealed by examining the molecular recognition behavior of the macrocyclic polyethers **2** and **3** as docking sites. When MOF-1001 crystals were introduced into a saturated solution of PQT·2PF$_6$ in acetone, the crystals immediately turned red, and the color intensified over 60 min (*21*) (Fig. 4, A to E, and movie S1)—a typical behavior for this binding event that indicates charge-transfer interactions (*22*) between PQT^{2+} and crown ether rings. This observation points to the formation of MOF-1001 pseudorotaxanes (*23*) by threading of PQT^{2+} through the middle of the crown ether. The reversibility of such a process was evidenced by the reappearance of the original light yellow color upon rinsing with acetone, where 60% of PQT^{2+} could be removed after rinsing MOF-1001 pseudorotaxanes (2.8 mg) four times with 1 ml every 30 min (*14*). The complexed MOF-1001 maintained the original high crystallinity of the parent framework, as confirmed by coincident powder x-ray diffraction patterns.

Further evidence of complexation was obtained by examining the ^{1}H nuclear magnetic resonance (NMR) spectrum of the MOF-1001 pseudorotaxanes after dissolution in DCl (*14*). Integration of the peaks appearing at 7.96 ppm (d, 4H, Ar-H^a in **2**, ^3J = 8.5 Hz; Fig. 4F) and 4.60 ppm (s, 6H, N-CH$_3$ in PQT^{2+}) revealed the expected 1:1 ratio of strut **2** and PQT^{2+}, indicating that the docking phenomenon of PQT^{2+} does indeed take place at every crown ether ring throughout the whole MOF framework (fig. S10). Solid-state ^{15}N NMR spectroscopy—a technique that is highly sensitive to the environment of the nitrogen (^{15}N) in PQT^{2+}—provided further evidence for docking in MOF-1001. Isotope-labeled PQT^{2+} (*14*) with 25% abundance of ^{15}N was used to make the MOF-1001 pseudorotaxanes, and the resulting solid was examined by ^{15}N cross-polarization magic angle spinning (CP/MAS) spectroscopy (*24*). The spectrum of the uncomplexed PQT^{2+} has a ^{15}N signal centered on 207.2 ppm, whereas the spectrum of PQT^{2+} bound within the crown ether rings in MOF-1001 shows an upfield shift to 204.6 ppm for the ^{15}N resonance resulting from docking into the macrocyclic polyether units of the struts (Fig. 4G).

Similar studies carried out on strut **2** were used as a molecular analog for comparison with MOF-1001 complexation experiments. Here, addition of PQT·2PF$_6$ to an acetone solution of strut **2** led to the formation of a pseudorotaxane, [PQT⊂**2**]·2PF$_6$. The binding affinity (K_a = 829 M^{-1}) (fig. S2) between PQT^{2+} and strut **2** in solution was obtained from spectrophotometric titrations. Single-crystal x-ray diffraction of the [PQT⊂**2**]·2PF$_6$ (Fig. 4H) clearly shows the insertion of the π-electron–deficient bipyridinium dication through the middle of the macrocyclic polyether. π-π stacking and [C–H···O] interactions are reflected in the interplanar separation of 3.6 Å between the bipyridinium unit of PQT^{2+} and the hydroquinone rings. The same upfield shift trend in the ^{15}N NMR spectra observed for MOF-1001 pseudorotaxanes was also evident in the ^{15}N NMR spectra of [PQT⊂**2**]·2PF$_6$ in the solid state (*14*) (Fig. 4I) as well as in solution (fig. S5). Control experiments were carried out by attempting to introduce PQT·2PF$_6$ into porous MOF-177 crystals (*25*), the pore dimensions (d = 11.8 Å) of which were expected to allow the free movement of PQT^{2+} within the pores. We found that fewer than 0.06 PQT^{2+} molecules per strut of MOF-177 were incorporated in the pores (fig.

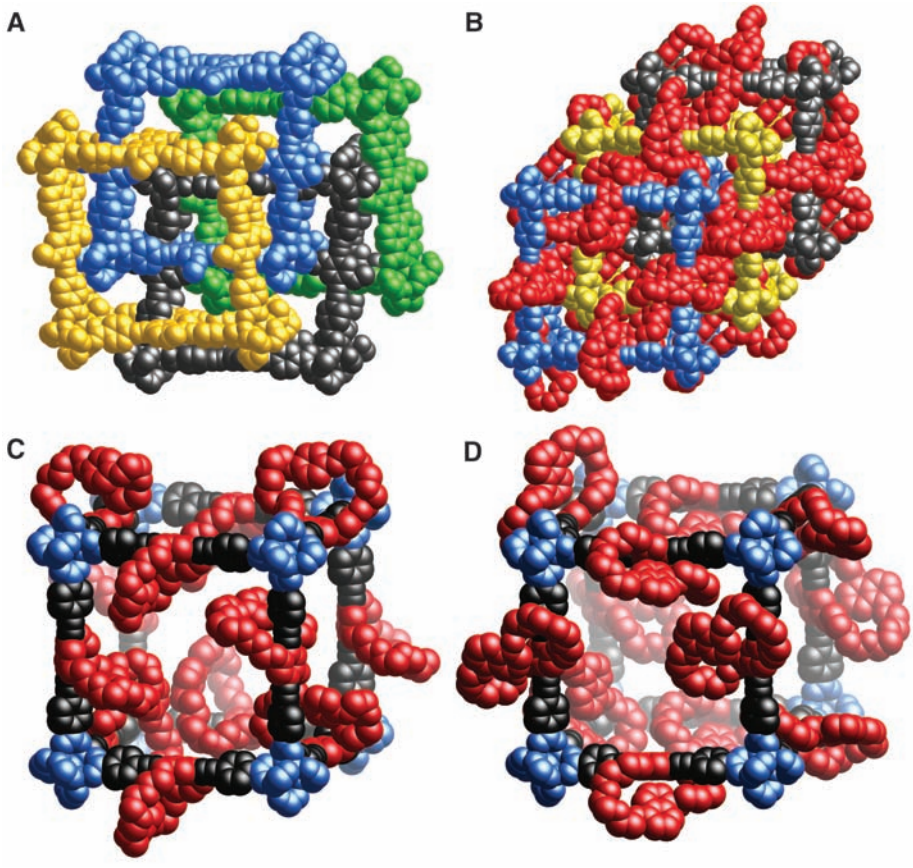

Fig. 3. Space-filling illustration of MOF-1000, MOF-1001A, MOF-1001, and MOF-1002. (**A** and **B**) The length of the struts (19.3 Å) allows the structures of MOF-1000 (A) and MOF-1001A (B) to interpenetrate. (**C** and **D**) In contrast, high volumes of open space were present in the noninterpenetrating MOF-1001 (C) and MOF-1002 (D) synthesized from struts with the same length. This feature ensures the full accessibility of the electron-donating receptors for the incoming substrates within the pores. The same color codes as in Fig. 2 were applied. All hydrogen atoms have been omitted for clarity.

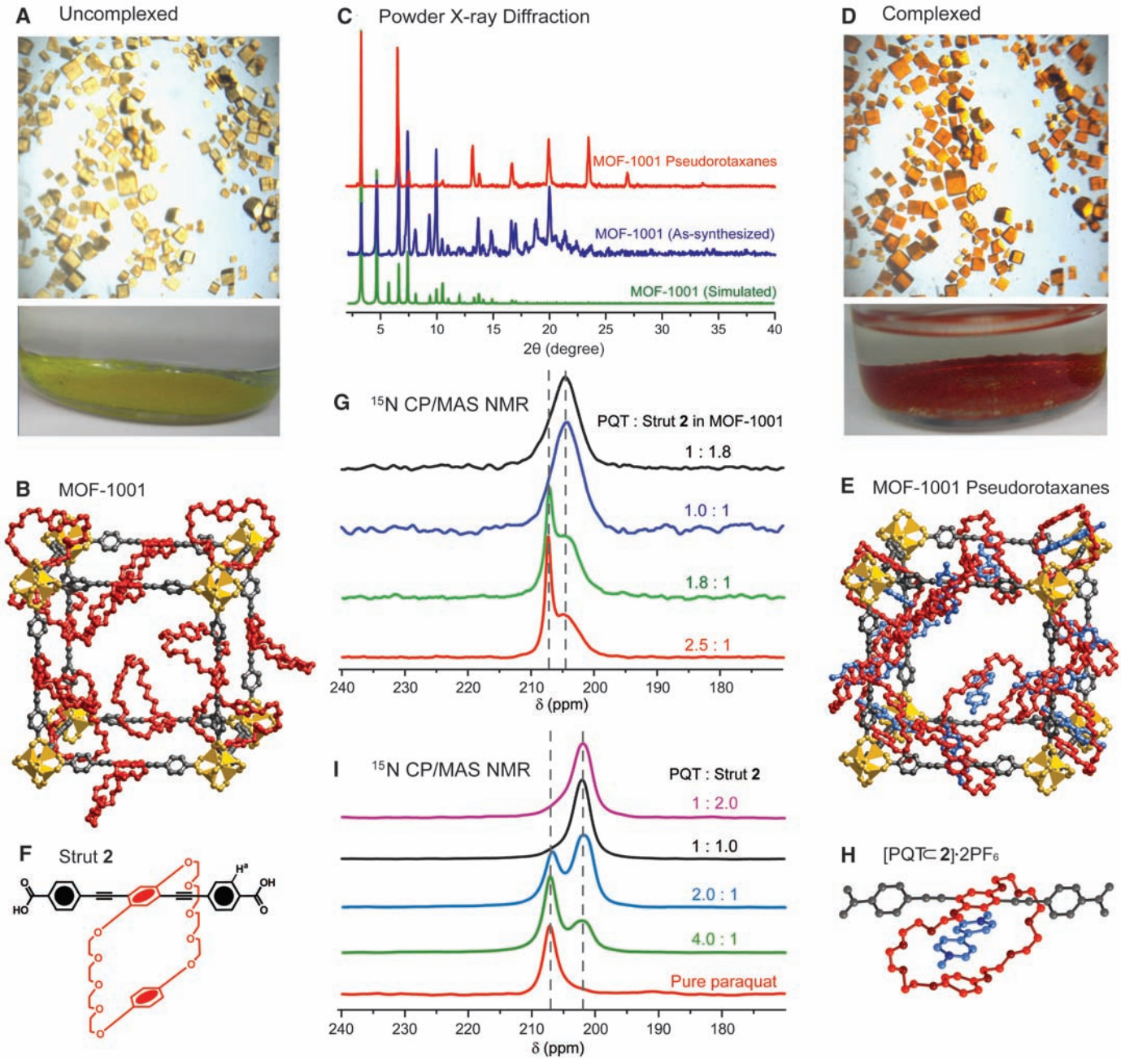

Fig. 4. X-ray diffraction and solid-state NMR spectroscopic studies on MOF-1001, MOF-1001 pseudorotaxanes, and their molecular analogs. (**A** to **C**) MOF-1001 [(A) and (B)] maintained its crystallinity after docking of PQT^{2+}, a single crystal–to–single crystal transformation revealed by the x-ray diffraction pattern (C). Dimensions of the cubic crystals varied from 0.05 to 0.45 mm. (**D** to **F**) This quantitative threading to form MOF-1001 pseudorotaxanes [(D) and (E)] was confirmed by the 1:1 stoichiometry of PQT^{2+} and strut **2** (F). The crystal structure of MOF-1001 and the simulated MOF-1001 pseudorotaxanes structure are illustrated in ball-and-stick models. (**G**) This docking phenomenon resulted in the upfield shifts of the ^{15}N CP/MAS signals (*11*) relative to free PQT^{2+}. (**H** and **I**) The molecular pseudorotaxane analog [PQT⊂**2**]·$2PF_6$ (H) was found to have the same upfield shift trend (I) ($\Delta\delta$ = 4.9 ppm). Color code: $Zn_4O(CO_2)_6$ polyhedra, gold; organic struts, gray; crown ethers, red; PQT^{2+}, blue. All hydrogen atoms and counterions have been omitted for clarity.

S11). These results clearly show that specific stereoelectronic host-guest interactions, rather than simple diffusion and adsorption, are responsible for the all but quantitative formation of the MOF-1001 pseudorotaxanes.

References and Notes

1. O. M. Yaghi *et al.*, *Nature* **423**, 705 (2003).
2. S. Kitagawa, R. Kitaura, S. Noro, *Angew. Chem. Int. Ed.* **43**, 2334 (2004).
3. G. Férey *et al.*, *Science* **309**, 2040 (2005).
4. A. G. Wong-Foy, A. J. Matzger, O. M. Yaghi, *J. Am. Chem. Soc.* **128**, 3494 (2006).
5. M. Eddaoudi *et al.*, *Science* **295**, 469 (2002).
6. Z. Wang, S. M. Cohen, *Chem. Soc. Rev.* **38**, 1315 (2009).
7. J. Lee *et al.*, *Chem. Soc. Rev.* **38**, 1450 (2009).
8. J. L. C. Rowsell, E. C. Spencer, J. Eckert, J. A. K. Howard, O. M. Yaghi, *Science* **309**, 1350 (2005).
9. J.-M. Lehn, *Science* **227**, 849 (1985).
10. J. F. Stoddart, *Nat. Chem.* **1**, 14 (2009).
11. H. Li, M. Eddaoudi, M. O'Keeffe, O. M. Yaghi, *Nature* **402**, 276 (1999).
12. We assign the MOF-1000 numbering scheme to MOFs that are constructed from struts capable of stereoelectronically controlled binding.
13. D. B. Amabilino, J. F. Stoddart, *Chem. Rev.* **95**, 2725 (1995).
14. See supporting material on *Science* Online.
15. Strut **1** was synthesized (*14*) by the attachment of 4-(carboxyphenyl)ethynyl groups to the 2- and 5-positions of a central 1,4-dimethoxybenzene ring using the Pd-catalyzed alkyne-aromatic Sonogashira coupling (*26*).
16. It has not escaped our attention that the phenylene rings that incorporate the struts in **2** and **3** also support planes of chirality. As a consequence, there is yet another fundamental

source of disorder associated with the polyether loops in MOF-1001A, MOF-1001, and MOF-1002. Moreover, there is also the prospect of being able to construct chiral MOFs where the elements of chirality are planar (*27*) in origin.
17. V. Balzani, A. Credi, F. M. Raymo, J. F. Stoddart, *Angew. Chem. Int. Ed.* **39**, 3348 (2000).
18. S. J. Loeb, *Chem. Commun.* **2005**, 1511 (2005).
19. K. Kim, *Chem. Soc. Rev.* **31**, 96 (2002).
20. C.-F. Lee *et al.*, *Nature* **458**, 314 (2009).
21. Crystals of MOF-1001 were first immersed in acetone to exchange the *N*,*N*-dimethylformamide (DMF) guests and unreacted BPP34C10DA. This process was repeated nine times by decanting and refreshing with acetone (5 ml) every 30 min to ensure full exchange of DMF.
22. D. B. Amabilino *et al.*, *J. Am. Chem. Soc.* **117**, 11142 (1995).
23. P. R. Ashton, D. Philp, N. Spencer, J. F. Stoddart, *J. Chem. Soc. Chem. Commun.* **23**, 1677 (1991).
24. The experiments were done by introducing acetone-exchanged MOF-1001 into acetone solutions of PQT·2PF_6 with different amounts of PQT^{2+}. After sitting for 6 hours, solvent was then removed by evaporation and the residue was further dried under vacuum (10^{-2} torr) overnight at room temperature. A ^{15}N CP/MAS NMR spectrum was acquired on the solid sample and the loading of PQT^{2+} was determined by solution-state ^{1}H NMR spectroscopy after digestion of the solid. See (*14*).
25. H. K. Chae *et al.*, *Nature* **427**, 523 (2004).
26. K. Sonogashira, Y. Tohda, N. Hagihara, *Tetrahedron Lett.* **16**, 4467 (1975).
27. V. Prelog, G. Helmchen, *Angew. Chem. Int. Ed. Engl.* **21**, 567 (1982).
28. This work was supported by the U.S. Department of Defense (Defense Threat Reduction Agency grant HDTRA1-08-10023) and Northwestern University. We thank S. Kabehie for assistance with emission spectroscopy. Crystallographic data for [PQT⊂**2**]·2PF_6, MOF-1000, MOF-1001A, MOF-1001, and MOF-1002 have been deposited into the Cambridge Crystallographic Data Centre under deposition numbers CCDC 728413 to 728420.

Supporting Online Material

www.sciencemag.org/cgi/content/full/325/5942/855/DC1
Materials and Methods
Figs. S1 to S24
Tables S1 to S11
Schemes S1 to S13
References
Movie S1

27 April 2009; accepted 19 June 2009
10.1126/science.1175441

Fire As an Engineering Tool of Early Modern Humans

Kyle S. Brown,[1,2] Curtis W. Marean,[2] Andy I. R. Herries,[3,4] Zenobia Jacobs,[5] Chantal Tribolo,[6] David Braun,[1] David L. Roberts,[7] Michael C. Meyer,[5] Jocelyn Bernatchez[2]

The controlled use of fire was a breakthrough adaptation in human evolution. It first provided heat and light and later allowed the physical properties of materials to be manipulated for the production of ceramics and metals. The analysis of tools at multiple sites shows that the source stone materials were systematically manipulated with fire to improve their flaking properties. Heat treatment predominates among silcrete tools at ~72 thousand years ago (ka) and appears as early as 164 ka at Pinnacle Point, on the south coast of South Africa. Heat treatment demands a sophisticated knowledge of fire and an elevated cognitive ability and appears at roughly the same time as widespread evidence for symbolic behavior.

There is debate as to when modern human behavior appeared, although there is increasing evidence for symbolic behavior by 80 to 70 thousand years ago (ka) (*1*, *2*) and perhaps earlier (*3*, *4*), during the African Middle Stone Age (MSA, ~280 to 35 ka) (*5*). The MSA also displays tool traits that anticipate technologies occurring later in Eurasia. This includes the regular and sometimes predominant use of blade technology (*4*), the production of unmodified and backed bladelets for probable use in composite tools (*6*), the refinement of bifacial technology, the production of formal and standardized tool types (*7*), and the use of refined bone tools (*8*). Although most raw materials during the MSA came from local nearby sources, early modern humans expanded their use of fine-grained raw materials (exotics) (*4*, *9*) from distant sources (*10*). The Still Bay [~71 to 70 ka (*11*) or earlier (*12*)] and Howiesons Poort (~65 to 60 ka) (*11*) MSA occurrences in South Africa display a preference for fine-grained materials, commonly silcrete [supporting online material (SOM) text] (*13*). The Still Bay occurrence has thin and symmetrical lanceolate and foliate shaped bifacials. The Howiesons Poort occurrence includes small retouched blade tools, along with the prepared-core and flake-and-blade technology typical of the MSA. The focus on silcrete has been argued to reflect functional need (*14*), increased mobility (*9*), trading networks (*15*), and even symbolic behavior (*16*).

Silcrete is traditionally described by archaeologists as a nonlocal fine-grained material that is highly workable in its natural state (*4*, *9*, *17*). However, our experimental replication using silcrete from sources on the south coast near Mossel Bay and Still Bay shows that these silcretes in their raw quarried form are difficult to flake consistently into formal tools. In Australia, indigenous knappers heated silcrete with fire (heat treatment) to improve the flaking quality of the material (*18*). Silcrete responds to heat treatment with significant improvement in workability and has a greater tolerance for high temperatures than do chert and flint (*19*). Following this lead, we found that heated South African silcrete is significantly more workable than unheated materials, and both bladelets and bifaces are easier to flake, with higher success rates. This transformation in workability is remarkably palpable when flaking both heated and unheated silcrete from the same source. Given these results, we undertook a systematic study of silcrete heat treatment and attempted to identify its presence or absence in the MSA.

We collected silcrete samples from sources located within 100 km of Pinnacle Point (*20*) (fig. S1). A witness control sample has been retained at our field laboratory in Mossel Bay, South Africa, for each nodule used in the experimental heat treatment study. Experimental silcrete samples were slowly heated to ~350°C in a scientific furnace or in sand beneath a fire pit (*20*).

The complexities of fracture mechanics make it difficult to quantify the workability of stone in a way that is relevant to human knapping (*21*). For this reason, we applied objective measures of workability and less objective but more realistic systematic flaking experiments. The rebound hardness test (*22*) assesses both the ability of a given rock mass to absorb energy and fracture predictability (SOM text). Rocks with internal flaws or low overall stiffness have lower rebound values (*23*). In these types of stones, the propagation of fracture will follow the internal structure of the rock rather than the direction of applied force. Heat-treated samples had significantly higher rebound hardness values (Wilcoxon matched-pairs test: $z = 2.512$, $P = 0.004$) than their paired untreated samples (fig. S2A and table S1) (*20*).

More carefully crafted bifacial tools have higher width-to-thickness ratios (W/T) (*24*), and variants of the W/T measurement correlate with projectile point function and ballistics (*25*). Timed heat-treated bifacial tool replications conducted by us had significantly higher W/T values [related-samples t test: $t(49) = 8.11$, $P < 0.001$] than their paired unheated bifaces (*20*). Using heated silcrete biface blanks, we could produce a significantly thinner biface that maximizes cutting edge, in the same amount of time needed to work the unheated bifaces (fig. S2, B and C). The heated biface samples closely resemble those of actual Still Bay point specimens (fig. S3). The rebound hardness and replication experiments combine to show that heat-treated silcretes consistently display more predictable fracture patterns, allowing

[1]Department of Archaeology, University of Cape Town, Rondebosch 7701, Cape Town, Republic of South Africa. [2]Institute of Human Origins, School of Human Evolution and Social Change, Post Office Box 872402, Arizona State University (ASU), Tempe, AZ 85287–4101, USA. [3]UNSW Archaeomagnetic Laboratory and Palaeosciences Laboratory, Integrative Palaeoecology and Anthropology Studies, School of Medical Sciences, University of New South Wales (UNSW), Kensington, New South Wales 2052, Australia. [4]Geomagnetism Laboratory, Department of Earth and Ocean Sciences, University of Liverpool, Liverpool L693BX, UK. [5]GeoQuEST Research Centre, School of Earth and Environmental Sciences, University of Wollongong, Wollongong 2522, Australia. [6]Institut de Recherche sur les Archéomatériaux–Centre de Recherche en Physique Appliquée à l'Archéologie, CNRS-Université de Bordeaux, Maison de l'Archéologie, Esplanade des Antilles, 33607 Pessac, France. [7]Council for Geoscience, Post Office Box 572, Bellville 7535, Republic of South Africa.